Ionics (2022) 28:1143–1155
https://doi.org/10.1007/s11581-021-04332-2

ORIGINAL PAPER

Analytical modeling of Li-ion diffusion in a three-layer electrode-separator-electrode stack with time-dependent current

Long Zhou[1,2] · Mohammad Parhizi[2] · Manan Pathak[3] · Ankur Jain[2]

Received: 28 April 2021 / Revised: 14 September 2021 / Accepted: 13 October 2021 / Published online: 4 January 2022

Abstract

Li-ion diffusion in electrodes and separator plays a key role in determining the charge/discharge characteristics of a Li-ion cell. Past papers have analyzed solution-phase limitation diffusion in a Li-ion cell for constant current conditions. In the present work, an analytical model is presented for concentration diffusion under solution-phase limitation in a three-layer structure under arbitrary, time-dependent current conditions that may be encountered in practical scenarios. The eigenvalue-based solution is shown to agree well with numerical simulations and may be suitable for implementation in practical battery management systems since only a few eigenvalues are shown to offer excellent accuracy. Computed concentration distributions are analyzed for sinusoidal and step function current profiles. The impact of electrode porosities on concentration distribution is also investigated. This work improves the theoretical understanding of diffusion in Li-ion cells and offers practical tools for modeling and optimization of electrochemical energy conversion and storage devices.

Keywords Concentration diffusion · Li-ion cell · Solution-phase limitation · Theoretical modeling

Nomenclature

$Brugg$	Bruggeman coefficient
c_i	Concentration in region i (mol m^{-3})
$c_{i,in}$	Initial concentration (mol m^{-3})
C_i	Dimensionless concentration in region i
$C_{i,in}$	Dimensionless initial concentration in region i
c_0	Reference concentration (mol m^{-3})
D	Diffusion coefficient of lithium ions in the electrolyte (m^2 s^{-1})
$D_{eff,i}$	Effective diffusion coefficient of lithium ions in each layer (m^2 s^{-1})
F	Faraday's constant (C mol^{-1})
i_{app}	Applied current density (A m^{-2})
J_i	Dimensionless flux density in region i
K	Ratio of electrode thicknesses
L	Total width of cell (m)
t	Time (s)
t_+	Transference number
x	Position (m)
ε_i	Porosity in region i
γ_i	Dimensionless position at the interface i
λ_n	Eigenvalue
τ	Dimensionless time
ξ	Dimensionless position

✉ Ankur Jain
jaina@uta.edu

[1] School of Mechanical and Power Engineering, Henan Polytechnic University, Jiaozuo, Henan, China

[2] Mechanical and Aerospace Engineering Department, University of Texas at Arlington, 500 W First St, Rm 211, Arlington, TX 76019, USA

[3] BattGenie, Inc., Seattle, WA, USA

Introduction

Mathematical modeling of Li-ion cells operating under different conditions is critical for performance prediction and design optimization [1–3]. In general, mathematical models for describing the behavior of Li-ion cells can be categorized as empirical or electrochemical models [2]. Electrochemical models are more sophisticated and provide detailed insights on multiple transport phenomena and kinetics occurring inside the cell [2, 4, 5]. Electrochemical models are based on solutions of governing equations for Li-ion concentration in solid and solution phase, intercalation reactions, and electrode potential in each phase [6–8].

One of the earliest and most extensively used electrochemical models for Li-ion batteries is the pseudo-2D (P2D) model, originally proposed by Doyle et al. [8–11]. P2D model is based on porous electrode theory [12] and the

concentrated solution theory [13], and it represents mass and charge transport, kinetics, and thermodynamics in both solid phase and the electrolyte [4, 14, 15]. However, P2D model is highly non-linear and coupled in nature since the concentration and potential fields in both electrodes and electrolyte are interrelated and must be solved simultaneously [16]. At low to moderate discharge rates or in sufficiently thin electrodes, a simplified version of P2D model known as single particle model (SPM) has been proposed [17–19]. In SPM, the dynamics of the solution phase is completely neglected, the entire electrode is represented by a single particle, and the solid phase diffusion becomes dominant [2, 20]. The assumptions associated with SPM do not hold at high discharge rates or for thick electrodes, where the concentration gradient in the electrolyte cannot be ignored anymore.

Due to the non-linear and coupled nature of the equations involved, exact solutions exist only for a few simplified problems and limiting operating cases. For example, Doyle and Newman proposed three different limiting cases including solution-phase diffusion limitation, solid-phase diffusion limitation, and ohmically dominated cell [1]. For solution-phase diffusion limitation, they suggested decoupling the governing equations for concentration, potential, and current density by considering a certain form for distribution of the reaction rate [1]. The separation of variables (SOV) technique was used to solve for these limiting cases [1]. SOV has also been used to determine the concentration profile in solution-phase diffusion limitation in a single insertion electrode [21]. This work was later extended to a Li-ion cell with two insertion electrodes and a separator [22]. Mathematical model of solution-phase diffusion in single insertion electrode has also been presented using Green's function approach [23]. Integral transform method has been used to address solid-phase diffusion limitation in different geometries and solution-phase diffusion limitation in a single insertion electrode [24]. Laplace transformation technique has been also used to predict the Li-ion concentration under both solid and solution-phase diffusion limitation assumptions [25]. In addition to such exact solutions, a variety of approximate analytical solutions such as the Parabolic Profile (PP) method [26, 27], Electrode Averaged Model (EAM) [28], and Proper Orthogonal Decomposition (POD) [29] have also been proposed.

While there is a long history of solving multilayer diffusion problems for applications such as porous media [30] and semiconductor devices [31], using a variety of methods such as Laplace transforms [32], eigenvalue expansion [33], and Duhamel theorem [34], as well as semi-analytical methods [35], there is, in general, a lack of such work in the context of Li-ion cells, particularly in the presence of time-dependent current.

Most analytical models for diffusion processes in a Li-ion cell assume constant current conditions. Even though time-varying current can be handled by numerical tools, there is still a need for analytical models capable of accounting for time-dependent current. Such problems are encountered in realistic scenarios such as dynamic charge/discharge in electric vehicles, as well as sinusoidal/harmonic current profiles used in battery diagnostics and electrochemical impedance spectroscopy (EIS) [36]. While such time-dependence can potentially be handled by a numerical simulation, it is desirable to develop analytical models for a better fundamental understanding of the effect of time-dependent current. A few previous studies have presented analytical and approximate analytical solutions to such problems. For example, Duhamel's superposition method has been used to develop an approximate solution for porous electrode model [8, 9]. An approximate solution for solid-phase diffusion limitation has been presented by developing an approximate eigenfunction and estimating the truncation error [19]. An exact solution for solid-phase diffusion limitation in a spherical electrode particle has been developed using finite integral transform method [37]. Recently Green's function based solution has been presented for solution-phase diffusion limitation in a two-layer body [38] and for solid-phase diffusion limitation [39] undergoing a variety of time-dependent charge/discharge. Separation of variable technique has been used to solve solution-phase diffusion limitation in a single insertion electrode [40] with time-dependent current.

This paper presents an analytical model to predict concentration profile in a three-layer Li-ion cell sandwich comprising of a positive and a negative electrode with a separator in between. Solution-phase diffusion limitation originally presented by Doyle and Newman [1] is considered in this study, and solid phase diffusion is neglected because it occurs much faster than solution-phase diffusion. The importance of concentration gradient in the electrolyte and consequently solution-phase diffusion limitation has been highlighted in previous studies [1]. This work generalizes a previous study [22] by accounting for a time-dependent reaction rate. Separation of variables (SOV) technique is used to derive a solution for concentration profile in a cell operating under time-dependent discharge current, which results in a time-dependent reaction rate. Note that, similar to previous studies [1, 8, 22], it is assumed that the reaction rate is uniform throughout the cell. The analytical model developed in this study is verified against independent, finite-element numerical simulations. This paper presents a useful mathematical tool to predict the concentration profile for more general and realistic conditions, which may contribute towards improved design and control of Li-ion cells.

Analytical modeling

Dimensionless governing equations

Consider Li-ion diffusion in a three-layer geometry, as shown in Figure 1, where layers 1 and 3 are the positive and negative electrodes, respectively, and layer 2 is the separator. In this paper, similar to previous studies [1, 8, 22], only solution-phase diffusion is considered, and the solid-phase diffusion is neglected. The transference number t_+ is assumed to be constant, based on the ionic mobility being independent of concentration, as is commonly assumed in the battery modeling literature [1, 8, 12]. In general, the concentration and potential fields in an electrochemical system are coupled with each other. Specifically, the migration of ions due to the potential field as well as the variation of the pore wall flux with potential is to be considered in the concentration conservation equation. However, the migration term is zero in this case due to the constant transference number, t_+ [1, 8, 12], and the assumption of uniform reaction rate uncouples the concentration calculations from the potential field. Only diffusion of Li ions is modeled, as the concentration distribution of the anions can be obtained using the electroneutrality equations. Further, the impact of crystal structure and chemical composition on the rate of diffusion is neglected.

Let $c_i(x,t)$ and ε_i be the concentration and the porosity of the i^{th} layer, respectively, and x_{i-1} and x_i be the boundary coordinates of the i^{th} layer, respectively, where $x_0 = 0$. The initial concentration in the layers at $t = 0$ is given by $c_{i,\,in}(x)$.

Conservation equations governing the concentration fields in the three layers are given in the following form [8, 22]:

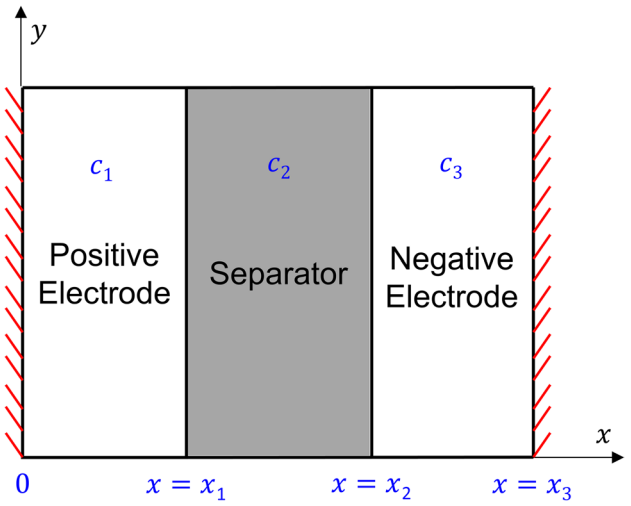

Fig. 1 Schematic of Li-ion cell comprising three regions – positive electrode, separator, and negative electrode

$$\varepsilon_1 \frac{\partial c_1}{\partial t} = D_{eff,1} \frac{\partial^2 c_1}{\partial x^2} - \frac{i_{app}(t)\left(1 - t_+\right)}{F\left(x_1 - x_0\right)} \quad (0 < x < x_1) \tag{1}$$

$$\varepsilon_2 \frac{\partial c_2}{\partial t} = D_{eff,2} \frac{\partial^2 c_2}{\partial x^2} \quad (x_1 < x < x_2) \tag{2}$$

$$\varepsilon_3 \frac{\partial c_3}{\partial t} = D_{eff,3} \frac{\partial^2 c_3}{\partial x^2} + \frac{i_{app}(t)\left(1 - t_+\right)}{F\left(x_3 - x_2\right)} \quad (x_2 < x < x_3) \tag{3}$$

where $i_{app}(t)$ is the time-dependent current density and F is Faraday's constant. Source terms in Eqs. (1) and (3) are based on charge balance assuming a constant and uniform pore wall flux [22].

Note that Eqs. (1)–(3) represent a balance between transient, diffusion, and generation/consumption terms. The migration term, which represents motion of charged species due to the imposed electric field [12], is not present in these equations, since the transference number t_+ is assumed to be independent of concentration [8].

Note that the diffusivities in each layer, $D_{eff,i}$, can be written in terms of D, the diffusion coefficient of Li ions in the electrolyte, and porosities of each layer as: $D_{eff,i} = D\varepsilon_i^{Brugg} \quad (i = 1, 2, 3)$. Therefore, the governing equations may be written as:

$$\varepsilon_1 \frac{\partial c_1}{\partial t} = D\varepsilon_1^{Brugg} \frac{\partial^2 c_1}{\partial x^2} - \frac{i_{app}(t)\left(1 - t_+\right)}{F\left(x_1 - x_0\right)} \quad (0 < x < x_1) \tag{4}$$

$$\varepsilon_2 \frac{\partial c_2}{\partial t} = D\varepsilon_2^{Brugg} \frac{\partial^2 c_2}{\partial x^2} \quad (x_1 < x < x_2) \tag{5}$$

$$\varepsilon_3 \frac{\partial c_3}{\partial t} = D\varepsilon_3^{Brugg} \frac{\partial^2 c_3}{\partial x^2} + \frac{i_{app}(t)\left(1 - t_+\right)}{F\left(x_3 - x_2\right)} \quad (x_2 < x < x_3) \tag{6}$$

Equations (4)–(6) represent a balance between diffusion and species consumption/generation due to the reaction in the electrodes. Note that there is no consumption/generation term in the equation for the separator since Li intercalation/de-intercalation occurs only in the electrodes.

Related boundary and interfacial conditions may be obtained from continuity of concentration and mass flux as follows:

$$\frac{\partial c_1}{\partial x} = 0 \quad (x = 0) \tag{7a}$$

$$\frac{\partial c_3}{\partial x} = 0 \quad (x = x_3) \tag{7b}$$

$$c_1 = c_2 \quad (x = x_1) \tag{7c}$$

$$\frac{\partial c_1}{\partial x} = \frac{\varepsilon_2^{Brugg}}{\varepsilon_1^{Brugg}} \frac{\partial c_2}{\partial x} \quad (x = x_1) \tag{7d}$$

$$c_2 = c_3 \quad (x = x_2) \tag{7e}$$

$$\frac{\partial c_2}{\partial x} = \frac{\varepsilon_3^{Brugg}}{\varepsilon_2^{Brugg}} \frac{\partial c_3}{\partial x} \quad (x = x_2) \tag{7f}$$

$$c_i = c_{i,in}(x) \quad (t = 0) \quad (i = 1, 2, 3) \tag{8}$$

Equations 7(a) and 7(b) represent zero flux at the two ends of the geometry where the electrodes come in contact with the current collector. Equations 7(c) and 7(e) represent species continuity at the two interfaces in the problem, while Eqs. 7(d) and 7(f) are obtained from mass flux balance at the interfaces.

For generality, the following dimensionless terms are introduced:

$$C_i = \frac{c_i}{c_0}; \xi = \frac{x}{L}; \gamma_i = \frac{x_i}{L}; \tau = \frac{Dt}{L^2} \tag{9}$$

where c_0 is a reference concentration and L is the total width of the three-layer structure.

Using Eq. (6), the following non-dimensional partial differential equations as well as the associated boundary and initial conditions are derived:

$$\varepsilon_1 \frac{\partial C_1}{\partial \tau} = \varepsilon_1^{Brugg} \frac{\partial^2 C_1}{\partial \xi^2} - J_1(\tau) \quad (0 < \xi < \gamma_1) \tag{10}$$

$$\varepsilon_2 \frac{\partial C_2}{\partial \tau} = \varepsilon_2^{Brugg} \frac{\partial^2 C_2}{\partial \xi^2} \quad (\gamma_1 < \xi < \gamma_2) \tag{11}$$

$$\varepsilon_3 \frac{\partial C_3}{\partial \tau} = \varepsilon_3^{Brugg} \frac{\partial^2 C_3}{\partial \xi^2} + K J_1(\tau) \quad (\gamma_2 < \xi < 1) \tag{12}$$

where $J_1 = \frac{i_{app}(\tau)(1-t_+)L}{F c_0 \gamma_1 D}$ is the non-dimensional current and $K = \frac{\gamma_1}{1-\gamma_2}$ is the ratio of electrode thicknesses.

The non-dimensional boundary conditions are:

$$\frac{\partial C_1}{\partial \xi} = 0 \quad (\xi = 0) \tag{13a}$$

$$\frac{\partial C_3}{\partial \xi} = 0 \quad (\xi = 1) \tag{13b}$$

$$C_1 = C_2 \quad (\xi = \gamma_1) \tag{13c}$$

$$\frac{\partial C_1}{\partial \xi} = \frac{\varepsilon_2^{Brugg}}{\varepsilon_1^{Brugg}} \frac{\partial C_2}{\partial \xi} \quad (\xi = \gamma_1) \tag{13d}$$

$$C_2 = C_3 \quad (\xi = \gamma_2) \tag{13e}$$

$$\frac{\partial C_2}{\partial \xi} = \frac{\varepsilon_3^{Brugg}}{\varepsilon_2^{Brugg}} \frac{\partial C_3}{\partial \xi} \quad (\xi = \gamma_2) \tag{13f}$$

$$C_i = C_{i,in}(\xi) \quad (\tau = 0) \quad (i = 1, 2, 3) \tag{14}$$

where $C_{i,in}(\xi) = \frac{c_{i,in}(x)}{c_0}$ is the non-dimensional initial condition. This completes the non-dimensional set of equations that needs to be solved in order to determine the concentration distribution in the three-layer electrode. Note that Eqs. (10)–(14) represent a generalization of a constant current model presented in the past [22]. Consideration of time-dependent currents in the present work has practical relevance due to time-varying loads encountered in electric vehicles. Accounting for such time dependence is theoretically non-trivial.

Solution method

Equations (10)–(14) represent a set of partial differential equations with homogeneous boundary and initial conditions. Equations (10) and (12) for the two electrodes contain non-homogeneous source terms.

In order to solve these equations, series forms are assumed for the concentration fields $C_1(\xi, \tau)$, $C_2(\xi, \tau)$, and $C_3(\xi, \tau)$ as follows:

$$C_1(\xi, \tau) = \sum_{n=0}^{\infty} \phi_{1,n}(\xi)\, q_n(\tau) \quad (0 < \xi < \gamma_1) \tag{15}$$

$$C_2(\xi, \tau) = \sum_{n=0}^{\infty} \phi_{2,n}(\xi)\, q_n(\tau) \quad (\gamma_1 < \xi < \gamma_2) \tag{16}$$

$$C_3(\xi, \tau) = \sum_{n=0}^{\infty} \phi_{3,n}(\xi)\, q_n(\tau) \quad (\gamma_2 < \xi < 1) \tag{17}$$

where $\phi_{1,n}(\xi)$, $\phi_{2,n}(\xi)$, and $\phi_{3,n}(\xi)$ are the eigenfunctions for the first, second, and third layers, respectively, and $q_n(\tau)$ is a time-dependent function.

By inserting the forms of the solution in the boundary conditions, the eigenfunctions are found to be:

$$\phi_{1,n}(\xi) = \cos\left(\lambda_n \xi\right) \tag{18}$$

$$\phi_{2,n}(\xi) = \alpha_{2n} \sin\left(\mu_{2n} \xi\right) + \beta_{2n} \cos\left(\mu_{2n} \xi\right) \tag{19}$$

$$\phi_{3,n}(\xi) = \alpha_{3n} \sin\left(\mu_{3n} \xi\right) + \beta_{3n} \cos\left(\mu_{3n} \xi\right) \tag{20}$$

where

$$\mu_{2n} = \left(\frac{\varepsilon_1}{\varepsilon_2}\right)^{\frac{Brugg-1}{2}} \lambda_n \tag{21a}$$

$$\mu_{3n} = \left(\frac{\varepsilon_1}{\varepsilon_3}\right)^{\frac{Brugg-1}{2}} \lambda_n \tag{21b}$$

$$\alpha_{2n} = \cos\left(\lambda_n\gamma_1\right)\sin\left(\mu_{2n}\gamma_1\right) - \left(\frac{\varepsilon_1}{\varepsilon_2}\right)^{\frac{Brugg+1}{2}} \sin\left(\lambda_n\gamma_1\right)\cos\left(\mu_{2n}\gamma_1\right) \tag{22a}$$

$$\beta_{2n} = \left(\frac{\varepsilon_1}{\varepsilon_2}\right)^{\frac{Brugg+1}{2}} \sin\left(\lambda_n\gamma_1\right)\sin\left(\mu_{2n}\gamma_1\right) + \cos\left(\lambda_n\gamma_1\right)\cos\left(\mu_{2n}\gamma_1\right) \tag{22b}$$

$$\alpha_{3n} = \frac{\sin\left(\mu_{3n}\right)\left\{\cos\left(\lambda_n\gamma_1\right)\cos\left[\mu_{2n}\left(\gamma_2-\gamma_1\right)\right] - \left(\frac{\varepsilon_1}{\varepsilon_2}\right)^{\frac{Brugg+1}{2}} \sin\left(\lambda_n\gamma_1\right)\sin\left[\mu_{2n}\left(\gamma_2-\gamma_1\right)\right]\right\}}{\cos\left[\mu_{3n}\left(1-\gamma_2\right)\right]} \tag{22c}$$

$$\beta_{3n} = \frac{\cos\left(\mu_{3n}\right)\left\{\cos\left(\lambda_n\gamma_1\right)\cos\left[\mu_{2n}\left(\gamma_2-\gamma_1\right)\right] - \left(\frac{\varepsilon_1}{\varepsilon_2}\right)^{\frac{Brugg+1}{2}} \sin\left(\lambda_n\gamma_1\right)\sin\left[\mu_{2n}\left(\gamma_2-\gamma_1\right)\right]\right\}}{\cos\left[\mu_{3n}\left(1-\gamma_2\right)\right]} \tag{22d}$$

Further, using boundary conditions given by Eqs. (13a)–(13f), the eigenvalues λ_n can be shown to satisfy the following transcendental equation:

$$\tan\left(\lambda_n\gamma_1\right) = \frac{\tan\left[\mu_{2n}\left(\gamma_2-\gamma_1\right)\right] + \left(\frac{\varepsilon_3}{\varepsilon_2}\right)^{\frac{Brugg+1}{2}} \tan\left[\mu_{3n}\left(1-\gamma_2\right)\right]}{\left(\frac{\varepsilon_1}{\varepsilon_2}\right)^{\frac{Brugg+1}{2}}\left\{\left(\frac{\varepsilon_3}{\varepsilon_2}\right)^{\frac{Brugg+1}{2}} \tan\left[\mu_{3n}\left(1-\gamma_2\right)\right]\tan\left[\mu_{2n}\left(\gamma_2-\gamma_1\right)\right] - 1\right\}} \tag{23}$$

Finally, note that the orthogonality relationship for the eigenfunctions is given by:

$$\frac{1}{\varepsilon_1^{Brugg-1}}\int_0^{\gamma_1}\phi_{1,m}(\xi)\phi_{1,n}(\xi)d\xi + \frac{\varepsilon_2}{\varepsilon_1^{Brugg}}\int_{\gamma_1}^{\gamma_2}\phi_{2,m}(\xi)\phi_{2,n}(\xi)d\xi + \frac{\varepsilon_3}{\varepsilon_1^{Brugg}}\int_{\gamma_2}^{1}\phi_{3,m}(\xi)\phi_{3,n}(\xi)d\xi = \begin{cases} 0 & m \neq n \\ N_n & m = n \end{cases} \tag{24}$$

where the norm is given by:

$$N_n = \frac{1}{\varepsilon_1^{Brugg-1}}\int_0^{\gamma_1}\phi_{1,n}^2(\xi)d\xi + \frac{\varepsilon_2}{\varepsilon_1^{Brugg}}\int_{\gamma_1}^{\gamma_2}\phi_{2,n}^2(\xi)d\xi + \frac{\varepsilon_3}{\varepsilon_1^{Brugg}}\int_{\gamma_2}^{1}\phi_{3,n}^2(\xi)d\xi \tag{25}$$

Dividing the governing equations given by Eqs. (10), (11), and (12) by ε_1, ε_2, and ε_3, respectively, and introducing the assumed forms of the concentration fields given by Eqs. (15), (16), and (17) result in:

$$\sum_{n=0}^{\infty}\phi_{1,n}(\xi)\dot{q}_n(\tau) = \varepsilon_1^{Brugg-1}\sum_{n=0}^{\infty}\phi_{1,n}''(\xi)q_n(\tau) - \frac{J_1(\tau)}{\varepsilon_1} \quad (0<\xi<\gamma_1) \tag{26}$$

$$\sum_{n=0}^{\infty}\phi_{2,n}(\xi)\dot{q}_n(\tau) = \varepsilon_2^{Brugg-1}\sum_{n=0}^{\infty}\phi_{2,n}''(\xi)q_n(\tau) \quad (\gamma_1<\xi<\gamma_2) \tag{27}$$

$$\sum_{n=0}^{\infty}\phi_{3,n}(\xi)\dot{q}_n(\tau) = \varepsilon_3^{Brugg-1}\sum_{n=0}^{\infty}\phi_{3,n}''(\xi)q_n(\tau) + K\frac{J_1(\tau)}{\varepsilon_3} \quad (\gamma_2<\xi<1) \tag{28}$$

where $\phi_{1,n}''(\xi)$, $\phi_{2,n}''(\xi)$, and $\phi_{3,n}''(\xi)$ are separately the second-order derivatives of functions $\phi_{1,n}(\xi)$, $\phi_{2,n}(\xi)$, and $\phi_{3,n}(\xi)$ with respect to ξ, and $\dot{q}_n(\tau)$ is the derivative of function $q_n(\tau)$ with respect to τ.

Now, Eqs. (26)–(28) are multiplied by $\frac{1}{\varepsilon_1^{Brugg-1}}\phi_{1,m}(\xi)$, $\frac{\varepsilon_2}{\varepsilon_1^{Brugg}}\phi_{2,m}(\xi)$, and $\frac{\varepsilon_3}{\varepsilon_1^{Brugg}}\phi_{3,m}(\xi)$, respectively, integrated in their respective ranges and added up. Algebraic simplification using the principle of orthogonality results in a much-simplified ordinary differential equation for $q_n(\tau)$:

$$\dot{q}_n(\tau) + \lambda_n^2\varepsilon_1^{Brugg-1}q_n(\tau) = \chi_n J_1(\tau) \tag{29}$$

where

$$\chi_n = \frac{1}{N_n}\left[-\frac{1}{\varepsilon_1^{Brugg}}\int_0^{\gamma_1}\phi_{1,n}(\xi)d\xi + K\frac{1}{\varepsilon_1^{Brugg}}\int_{\gamma_2}^{1}\phi_{3,n}(\xi)d\xi\right] \tag{30}$$

In order to determine the initial condition for $q_n(\tau)$, Eqs. (15)–(17) are substituted in the initial conditions given by Eq. (14), which, with the use of the orthogonality relationship given by Eq. (24), results in:

$$q_n(0) = \frac{\frac{1}{\varepsilon_1^{Brugg-1}}\int_0^{\gamma_1} C_{in}(\xi)\phi_{1,n}(\xi)d\xi + \frac{\varepsilon_2}{\varepsilon_1^{Brugg}}\int_{\gamma_1}^{\gamma_2} C_{in}(\xi)\phi_{2,n}(\xi)d\xi + \frac{\varepsilon_3}{\varepsilon_1^{Brugg}}\int_{\gamma_2}^{1} C_{in}(\xi)\phi_{3,n}(\xi)d\xi}{N_n} \tag{31}$$

The ordinary differential equation for $q_n(\tau)$, given by Eq. (29) subject to the initial condition given by Eq. (31), has a straightforward solution given by

$$q_n(\tau) = q_n(0)e^{-\lambda_n^2\varepsilon_1^{Brugg-1}\tau} + \chi_n\int_0^{\tau} J_1(\tau^*)e^{\lambda_n^2\varepsilon_1^{Brugg-1}(\tau^*-\tau)}d\tau^* \tag{32}$$

This completes the solution. Substituting Eqs. (18), (19), and (20) into Eqs. (15), (16), and (17) separately, the analytical solutions for the concentration distribution are given by:

$$C_1(\xi,\tau) = \sum_{n=0}^{\infty}\cos\left(\lambda_n\xi\right)q_n(\tau) \quad (0 < \xi < \gamma_1) \tag{33}$$

$$C_2(\xi,\tau) = \sum_{n=0}^{\infty}\left[\alpha_{2n}\sin\left(\mu_{2n}\xi\right) + \beta_{2n}\cos\left(\mu_{2n}\xi\right)\right]q_n(\tau) \quad (\gamma_1 < \xi < \gamma_2) \tag{34}$$

$$C_3(\xi,\tau) = \sum_{n=0}^{\infty}\left[\alpha_{3n}\sin\left(\mu_{3n}\xi\right) + \beta_{3n}\cos\left(\mu_{3n}\xi\right)\right]q_n(\tau) \quad (\gamma_2 < \xi < 1) \tag{35}$$

Results and discussion

Number of eigenvalues needed

Since the solution for the concentration field defined by Eqs. (33)–(35) is in the form of an infinite series, it is important to examine the convergence of the series and determine the minimum number of eigenvalues needed for accurate computation of the concentration field. This is particularly important in this problem because of the need to compute the solution in the battery management system (BMS) of a Li-ion battery pack where only limited memory and computation resources may be available. Figure 2 plots concentration at $\xi = 0$ as a function of time for a problem with $\varepsilon_1 = 0.385$, $\varepsilon_2 = 0.724$, $\varepsilon_3 = 0.485$, $\gamma_1 = 0.414$, $\gamma_2 = 0.544$, and $Brugg = 4$. Results are plotted for constant current and time-dependent current conditions in Figure 2a and 2b, respectively. In each case, a number of curves are plotted with different number of eigenvalues used for computing the concentration field based on Eqs. (33)–(35). Both Figure 2a and 2b show that only a few number of eigenvalues is sufficient for convergence of the infinite series. There is negligible difference between the curves corresponding to 4 and 5 eigenvalues. In addition, even if only one eigenvalue is used, the maximum error (compared to the 5 eigenvalue case) is still less than 3.6% and 12.8% for the two cases considered here. This illustrates a significant advantage of the analytical model presented here compared to numerical simulations that are memory-intensive and may require specialized software. Even using a single term in Eqs. (33)–(35) may be sufficient within reasonable engineering accuracy. Note that the analysis presented in Figure 2 is specific to the parameters chosen, and similar investigation of convergence characteristics should ideally be carried out for the specific set of parameters to be expected in a particular application of the analytical model presented here.

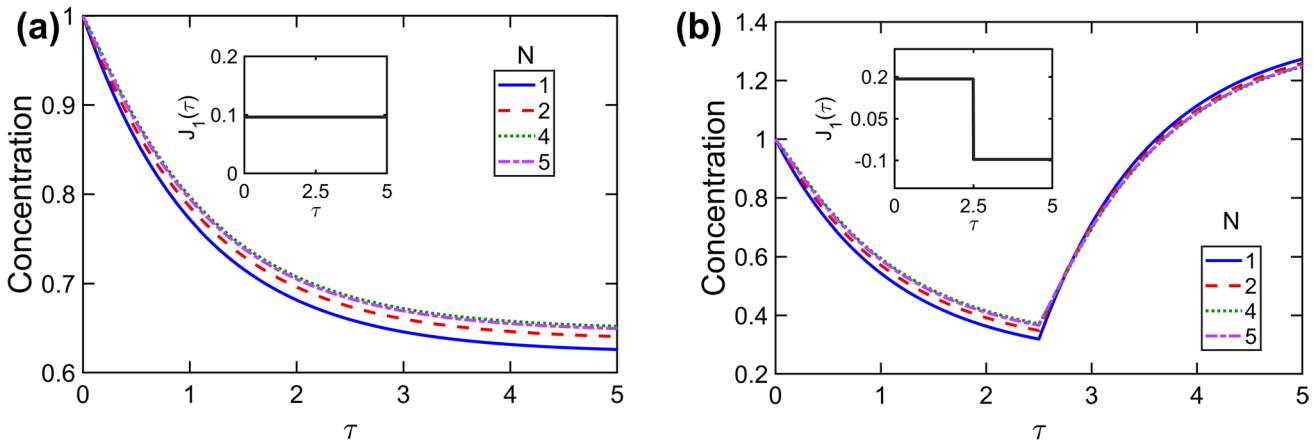

Fig. 2 Effect of number of eigenvalues: concentration as a function of τ at $\xi = 0$ for (**a**) constant reaction rate $J_1 = 0.09625$; (**b**) time-dependent current reaction rate, $J_1 = 0.1925$ if $0 < \tau < 2.5$ and $J_1 = -0.09625$ if $2.5 \le \tau < 5$

Model verification by comparison with numerical simulations

The analytical model presented in the previous section is verified by comparison with rigorous numerical simulations. A fully implicit finite difference method is used for solving the governing equations and boundary conditions defined in Eqs. (10)–(14). Equations are discretized in space and time in an implicit fashion. A total number of 1000 nodes are found to be sufficient in the one-dimensional geometry to ensure mesh independence. The non-dimensional time range is also divided into 1000 steps. Spatial discretization is carried out in such a way that a node is always assigned at each interface between layers. This helps implement interfacial requirements of continuity of concentration and flux. The resulting system of algebraic equations is solved using a tri-diagonal matrix algorithm (TDMA).

In the first comparison, a constant current density is considered in the three-layer geometry, with $\gamma_1 = 0.4$ and $\gamma_2 = 0.6$. Values of other parameters are $Brugg = 4$, $\varepsilon_1 = 0.385$, $\varepsilon_2 = 0.724$, and $\varepsilon_3 = 0.485$. Figure 3 compares the concentration field computed from Eqs. (33)–(35) with numerical simulation results for a constant current of $J_1 = 0.1925$. Figure 3a plots spatial distribution in concentration at three different times, and Figure 3b plots variation with time at the two ends ($\xi = 0$, 1) and two interfaces ($\xi = \gamma_1, \gamma_2$). Both figures show excellent agreement between the present work ad numerical simulations.

For further verification of the present model, results are compared with numerical simulations for a time-varying current boundary condition. A commonly encountered charge-rest-discharge scenario is modeled, wherein, the boundary flux $J_1 = 0.1925$ for $0 < \tau < 2$, $J_1 = 0$ for $2 < \tau < 3$, and $J_1 = -0.28875$ for $3 < \tau < 5$. The geometry and other properties are the same as Figure 3. For this set of parameters, Figure 4 plots and compares results from the present analytical model against numerical simulations. Figure 4a plots the concentration distribution at three different times, one each in the charge, rest, and discharge phases. Figure 4b plots concentration as a function of time at four locations in the cell. In both cases, there is very good agreement between the analytical model and numerical simulations. The maximum error between the two for Figure 4a and 4b is less than 1% in each case.

Model applications: sinusoidal current

Concentration distribution due to a sinusoidal current is studied next. An investigation of sinusoidal currents is carried out here because of the practical relevance of sinusoidal current profiles. An appropriate Fourier series expansion can be used to represent any general current profile with a series of sinusoidal terms. Therefore, responses to sinusoidal currents determined from the analytical model can be used to construct responses for any general function.

Two specific current profiles are considered. The first case considers $J_1(\tau) = 0.1925\, sin\,(2\pi\omega\tau)$, which represents a scenario where the cell cycles sinusoidally between charge and discharge at a frequency ω. For the same geometry and parameter values considered in Figure 2, the concentration field is computed for this sinusoidal current density and plotted in Figure 5. In particular, concentration is plotted as a function of time at the two ends, $\xi = 0$ and $\xi = 1$ in Figure 5a and 5b, respectively. In each case, curves for four different values of frequency, ω, are presented. As expected, for the plot at $\xi = 0$, the concentration starts by going down for

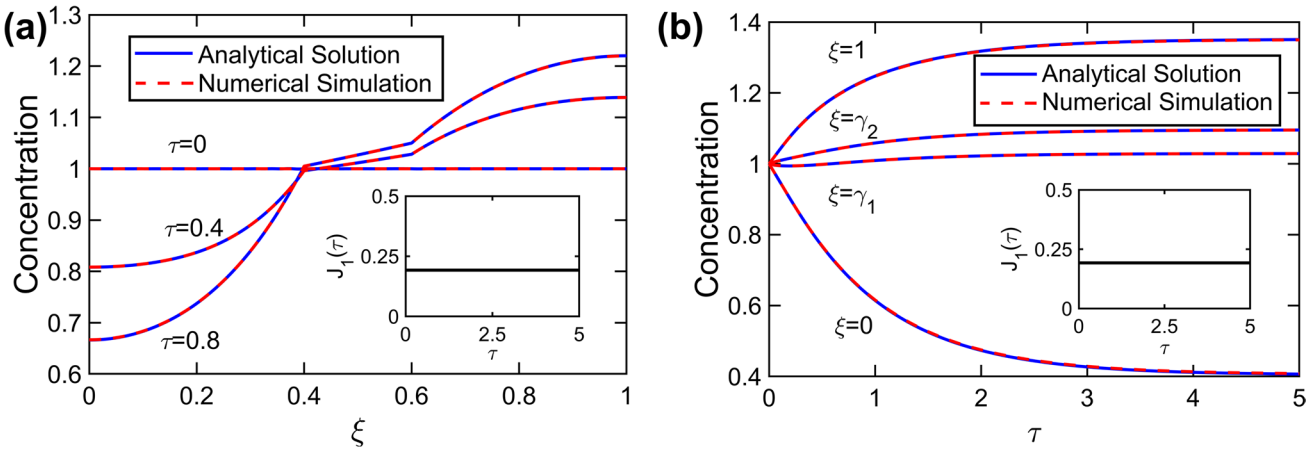

Fig. 3 Verification against numerical simulations for the special case of constant reaction rate, $J_1 = 0.1925$: (**a**) concentration as a function of ξ at $\tau = 0$, 0.4, 0.8; (**b**) concentration as a function of τ at $\xi = 0, \gamma_1, \gamma_2, 1$

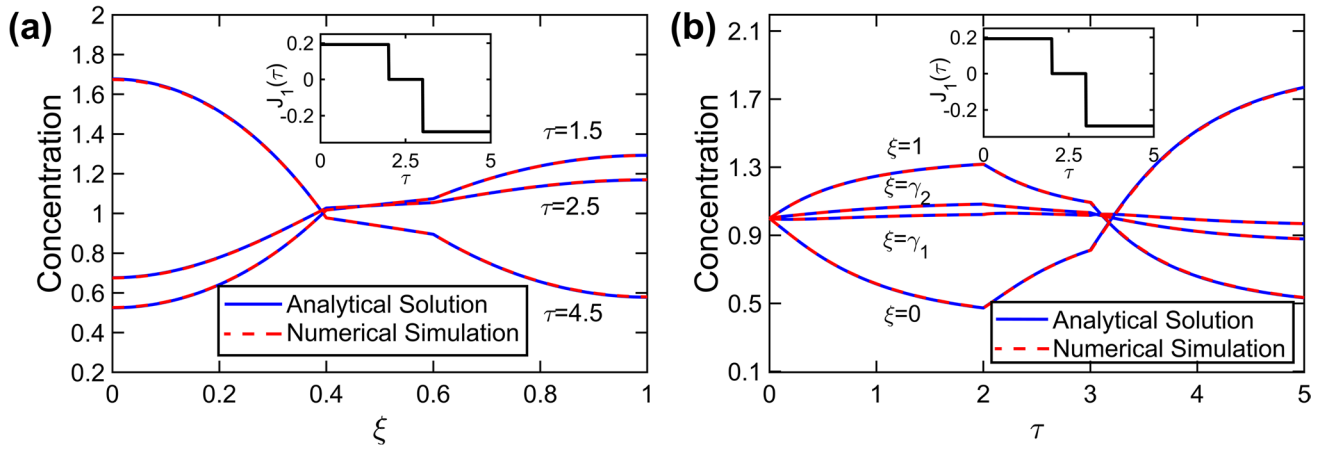

Fig. 4 Verification against numerical simulations for a time-dependent reaction rate, $J_1 = 0.1925$ if $0 < \tau < 2$, $J_1 = 0$ if $2 \leq \tau < 3$ and $J_1 = -0.28875$ if $3 \leq \tau < 5$: (**a**) concentration as a function of ξ at $\tau = 1.5$, 2.5, and 4.5; (**b**) concentration as a function of τ at $\xi = 0$, γ_1, γ_2, 1

each frequency, before rising and cycling a number of times according to the frequency for each case. In contrast, the concentration first rises for the plot at $\xi = 1$. This is consistent with the initially negative and positive values of the generation term in the first and third layer (Eqs. (10) and (12), respectively) for the given current profile. The amplitude of the concentration harmonics in Figure 5a and 5b reduce with increasing ω, which is because as the frequency increases, the current switches direction between charge and discharge much faster. Thus, the cell undergoes charge or discharge for a shorter period of time, leading to lower amplitude for the concentration. On average, there is a no significant change in the concentrations at $\xi = 0$ and $\xi = 1$, respectively, over the time period plotted in Figure 5. This is because based on the current profile, the cell spends an equal amount of time in charge and discharge over a cycle.

Results for a contrasting sinusoidal current profile are presented in Figure 6. In this case, $J_1(\tau) = 0.1925(1 + sin(2\pi\omega\tau))$, which represents a combination of constant and sinusoidal current. Unlike the previous problem, J_1 always remains non-negative and thus there is no discharge in this scenario. Concentration profiles at the two ends of the geometry, $\xi = 0$ and $\xi = 1$, are presented in Figure 6a and 6b, respectively. Similar to the previous figure, the concentrations at $\xi = 0$ and $\xi = 1$ vary sinusoidally, with an initial decrease and increase, respectively. This remains consistent with the sinusoidal nature of the charge profile. A key distinction in the concentration profiles in this case and the previous case is that there is an overall reduction and increase in concentrations at $\xi = 0$ and $\xi = 1$, respectively, over time. This is because, unlike the previous case, where the current profile comprised of both charge and discharge periods that,

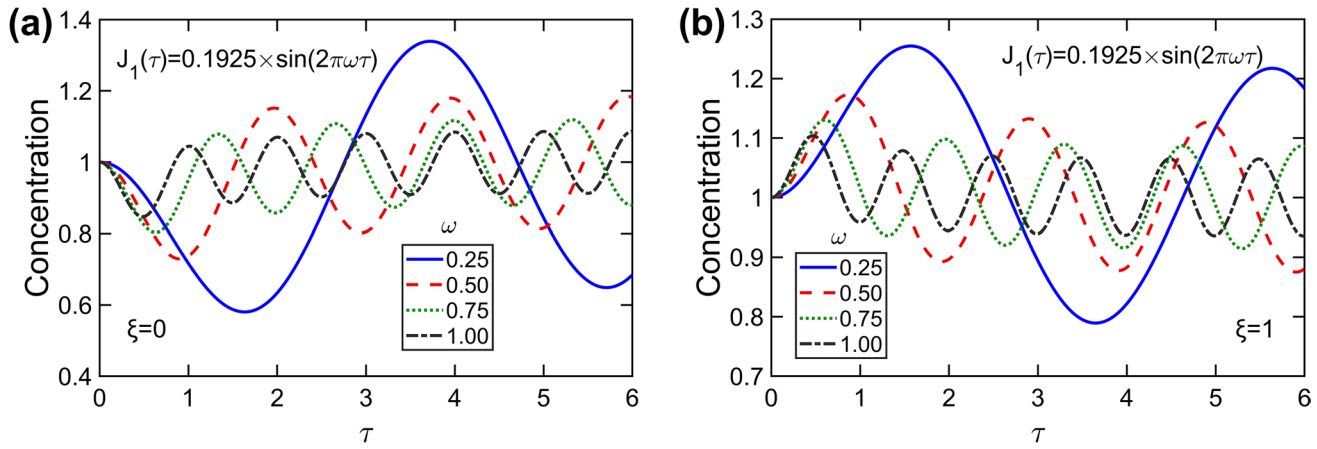

Fig. 5 Application of the model for a periodic reaction rate, $J_1(\tau) = 0.1925\, sin\,(2\pi\omega\tau)$: (**a**) concentration as a function of τ at $\xi = 0$ for $0 < \tau < 6$, (**b**) concentration as a function of τ at $\xi = 1$ for $0 < \tau < 6$ for $\omega = 0.25$, 0.5, 0.75, 1

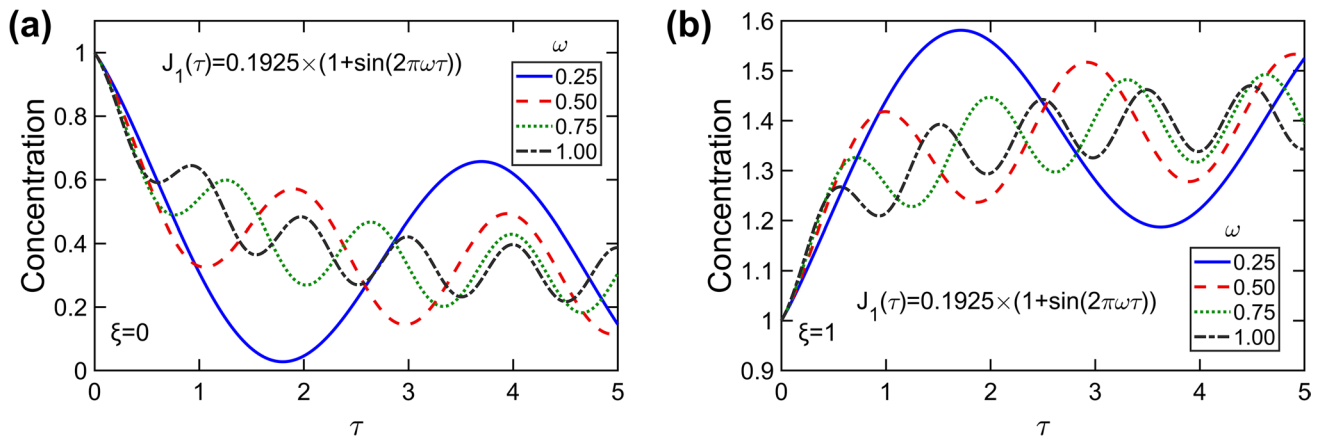

Fig. 6 Application of the model for a periodic reaction rate, $J_1(\tau) = 0.1925(1 + sin(2\pi\omega\tau))$: (**a**) concentration as a function of τ at $\xi = 0$ for $0 < \tau < 5$; (**b**) concentration as a function of τ at $\xi = 1$ for $0 < \tau < 5$ for $\omega = 0.25, 0.5, 0.75, 1$

on average, canceled each other out, in the present case, the current always remains non-negative, even though its value varies over time. This results in the cell getting charged over time, represented by the trends in concentration seen in Figure 6a and 6b over time.

Model applications: step function current

A step function current profile is also of practical relevance since sudden changes in charge/discharge in practical applications can be modeled as a step function. For example, sudden breaking or acceleration of an electric vehicle can, to the first order, be modeled as a step function change in the current profile. The impact of step changes in current on the concentration distribution is examined in Figure 7. Concentrations at $\xi = 0$ and $\xi = 1$ are plotted as functions of time for two different step functions. The case of an increasing step function, $J_1 = 0.0481$ if $0 \le \tau < 1$, $J_1 = 0.0.9625$ if $1 \le \tau < 3$ and $J_1 = 0.1925$ if $3 \le \tau < 5$, is presented in Figure 7a. A contrasting step function that decreases, then increases ($J_1 = 0.28875$ if $0 \le \tau < 1$, $J_1 = -0.385$ if $1 \le \tau < 3$, and $J_1 = 0.1925$ if $3 \le \tau < 5$), is presented in Figure 7b. In the first case, concentration at $\xi = 0$ monotonically decreases, while concentration at $\xi = 1$ monotonically increases through all three phases of the current profile. As expected, both curves become steeper as the current increases. In contrast, as shown in Figure 7b, when the current profile is such that current decreases, then increases, the concentration profiles are no more monotonic. Instead, concentration at $\xi = 0$ decreases, then increases, and then finally decreases, while concentration at $\xi = 1$ follows the opposite trend. On the overall, there is a slight reduction in concentration at $\xi = 0$

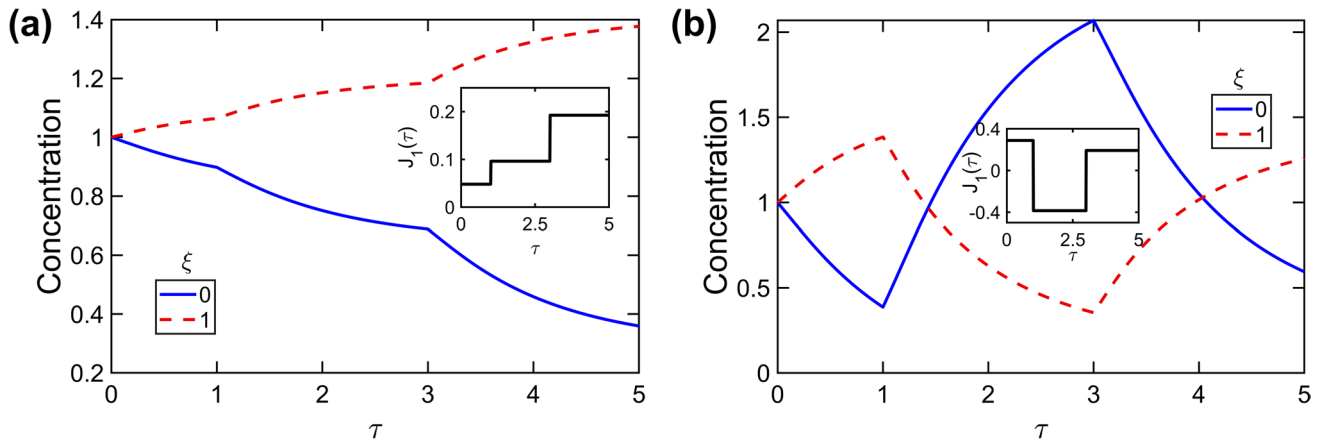

Fig. 7 Application of the model for step function reaction rate: concentration as a function of τ at $\xi = 0, 1$ for (**a**) $J_1 = 0.0481$ if $0 \le \tau < 1$, $J_1 = 0.09625$ if $1 \le \tau < 3$, and $J_1 = 0.1925$ if $3 \le \tau < 5$; (**b**) $J_1 = 0.28875$ if $0 \le \tau < 1$, $J_1 = -0.385$ if $1 \le \tau < 3$, and $J_1 = 0.1925$ if $3 \le \tau < 5$

and slight increase in concentration at $\xi = 1$ over the entire time period because of the net-charging nature of the specific current profile considered here.

Effect of electrode porosities

The porosities of the electrodes, ε_1 and ε_3, are key parameters of this diffusion problem. In order to determine the impact of porosities on concentration distribution in the cell, the concentration field is computed for a number of cases with varying values of the porosities.

Figure 8a and 8b plot concentration distributions in the three-layer structure at multiple times for two different values of ε_1 while all other parameters, including ε_2 and ε_3, are held constant. The concentration, initially uniform in each layer, becomes more and more distributed as time passes, as a result of diffusion. As seen from Eq. (10), a higher value of ε_1 results in reduced rate at which species distribution occurs due to diffusion. This is the reason why the concentration distributions in the first layer at various times are grouped closer in Figure 8b, where the value of ε_1 is greater than in Figure 8a, where the curves are farther apart due to the lower value of ε_1. Further, based on Eq. (7d), a higher value of ε_1 is expected to result in lower slope of the concentration distribution in the first layer at the interface with the second layer. This is also clearly seen in Figure 8a and 8b.

Further analysis of the impact of porosity values is presented in Figures 9 and 10. While keeping all other parameters constant, including ε_3, concentration is computed and plotted as function of space for five different values of ε_1 at two different times in Figure 8a and 8b, respectively. The current density is assumed to be a step function, with $J_1 = 0.1925$ for $0 < \tau < 2.5$ and $J_1 = 0.09625$ afterwards. The specific values of porosities in these plots are chosen to be

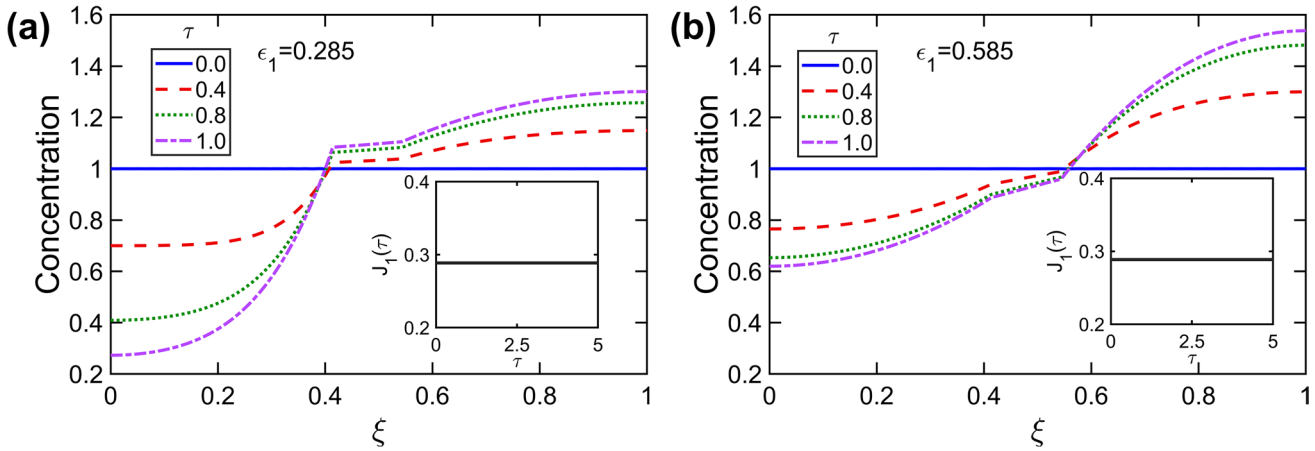

Fig. 8 Effect of porosity of the first layer. Concentration as a function of ξ at $\tau = 0$, 0.4, 0.8, and 1.0, with $J_1 = 0.28875$: (**a**) for $\varepsilon_1 = 0.285$, (**b**) $\varepsilon_1 = 0.585$. Other porosities and parameters are held constant

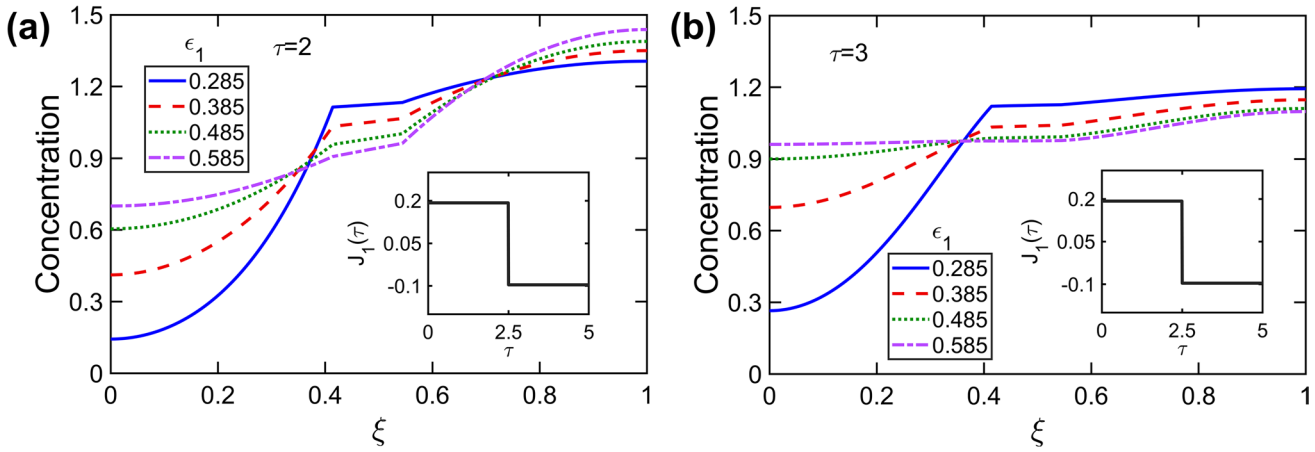

Fig. 9 Effect of porosity of the first layer. Concentration as a function of ξ for four different values of ε_1, with $J_1 = 0.1925$ if $0 < \tau < 2.5$ and $J_1 = -0.09625$ if $2.5 \leq \tau < 5$: (**a**) at $\tau = 2$, (**b**) at $\tau = 3$. Other porosities and parameters are held constant

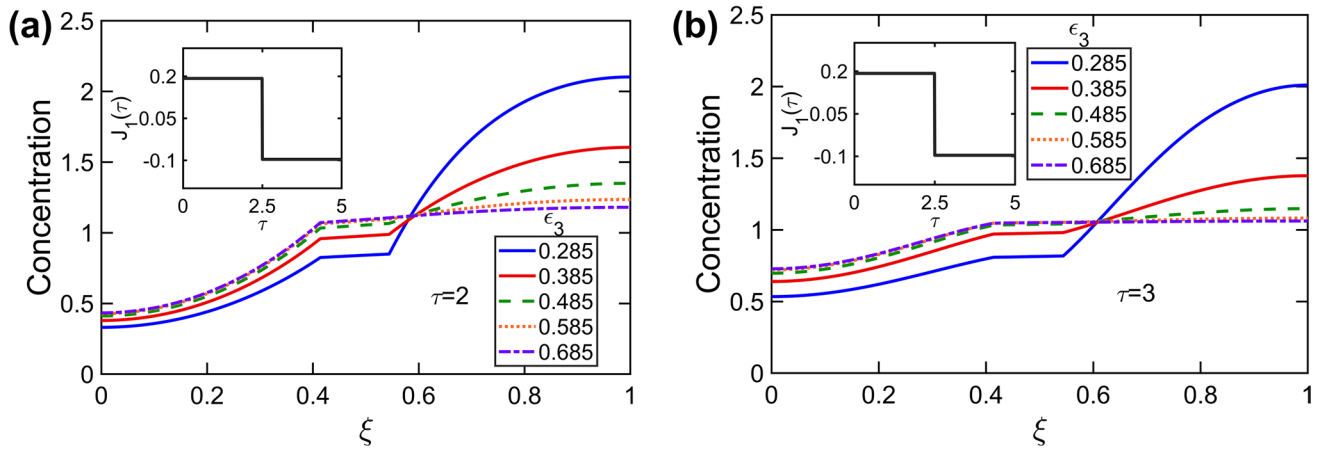

Fig. 10 Effect of porosity of the third layer. Concentration as a function of ξ for five different values of ε_3, with $J_1 = 0.1925$ if $0 < \tau < 2.5$ and $J_1 = -0.09625$ if $2.5 \leq \tau < 5$: (**a**) at $\tau = 2$, (**b**) at $\tau = 3$. Other porosities and parameters are held constant

consistent with past work [22]. As the value of ε_1 increases, Figure 9a shows reduced spatial gradient in the concentration distribution in the first layer, while the distribution in the third layer is relatively unaffected. This is consistent with greater rate of diffusion of species at low values of ε_1. A similar behavior is also observed at a later time shown in Figure 9b, when the current is lower due to the nature of the step function current profile. Consistent with Figures 8 and 9a, a greater gradient in concentration in the first layer is observed for a lower value of ε_1. Figure 9a also shows greater slope in concentration in the first layer at the interface with the separator at lower values of ε_1, as expected from Eq. (7d).

A similar analysis is carried out to investigate the impact of porosity of the other electrode, ε_3. Results are plotted in Figure 10a and 10b in the form of concentration distributions at two different times for different values of ε_3. As expected, in this case, since ε_3 is being varied, the impact of varying ε_3 is seen predominantly in the concentration distribution in the third layer, with greater concentration gradient at lower value of ε_3. There is relatively lesser impact of changing ε_3 on concentration distribution. Similar to Figure 9, the concentration distribution in the third layer becomes broader as the value of ε_3 decreases. In addition, a smaller value of ε_3 also results in a greater slope at the interface between the second and third layers.

Conclusions

Accurate modeling of concentration diffusion in multilayer Li-ion cells, such as electrode-separator-electrode stack, is critical for understanding and optimizing the overall performance of the system. While past work is available for constant current conditions, this work presents a model for a more realistic condition where the applied current may vary with time, including switch between charge and discharge. Such models may be applicable in several practical scenarios, such as in electric vehicles, where the electrical load on the battery varies widely over time, and therefore, the direct application of constant current models is not valid. It must be noted that the model presented above is valid in the solution-phase limitation, where diffusion within solid particles in the electrode may be neglected. The importance of solution-phase diffusion limitation has been highlighted in previous studies [1, 21, 22]. Also, the present analysis may break down at high currents and thick electrodes since the constant reaction rate assumption may not be valid in such cases. Further, the present model neglects the dependence of diffusion coefficients and transference number on concentration. Such non-linear effects are often difficult to capture in analytical models and may also not be significant in several practical scenarios. Finally, the present model is isothermal, and temperature effects on problem parameters have been neglected. Several of these assumptions are reasonably valid in practical applications, and therefore, the results presented here may be of practical relevance. Further, it must be noted that the theoretical framework developed here helps provide insights into the physics of the problem that may not be possible through numerical simulations and that the theoretical framework may be useful as a starting point for solving more complicated problems such as those with concentration-dependent reaction rate [41].

By showing that only a few number of eigenvalues offer reasonable accuracy in results, this work offers a practical method to compute concentration diffusion problems in practical electrochemical systems. Specifically, the analytical model can be computed using limited computing capabilities available in battery management systems, compared to numerical simulations. It is expected that the results

presented here may help improve our capability to model, analyze, and optimize the performance of practical electrochemical energy conversion and storage systems.

Author contribution Long Zhou – Methodology, formal analysis, investigation, data curation, visualization; Mohammad Parhizi – Methodology, formal analysis, investigation, data curation, visualization; Manan Pathak – Conceptualization, methodology, visualization, funding acquisition; Ankur Jain – conceptualization, methodology, supervision, project administration, visualization, funding acquisition. All authors contributed towards writing original draft and review/editing.

Funding This material is based upon work supported by CAREER Award No. CBET-1554183 from the National Science Foundation. This research was also supported by the Key Project of Science of the Education Bureau of Henan Province (19B460005), the Special Project of Basic Scientific Research Operating Expenses of Henan Polytechnic University (NSFRF180427), and the China Scholarship Council.

Data availability Data and material are available upon request from the corresponding author.

Code availability Code is available upon request from the corresponding author.

Declarations

Conflict of interest/Competing interests The authors declare no competing interests.

References

1. Doyle M, Newman J (1997) Analysis of capacity–rate data for lithium batteries using simplified models of the discharge process. J Appl Electrochem 27:846–856. https://doi.org/10.1023/A:1018481030499
2. Jokar A, Rajabloo B, Désilets M, Lacroix M (2016) Review of simplified pseudo-two-dimensional models of lithium-ion batteries. J Power Sources 327:44–55. https://doi.org/10.1016/j.jpowsour.2016.07.036
3. Zhang J, Lee J (2011) A review on prognostics and health monitoring of Li-ion battery. J Power Sources 196:6007–6014. https://doi.org/10.1016/j.jpowsour.2011.03.101
4. Ramadesigan V, Northrop PWC, De S, Santhanagopalan S, Braatz RD, Subramanian VR (2012) Modeling and simulation of lithium-ion batteries from a systems engineering perspective. J Electrochem Soc 159. https://doi.org/10.1149/2.018203jes
5. Seaman A, Dao TS, McPhee J (2014) A survey of mathematics-based equivalent-circuit and electrochemical battery models for hybrid and electric vehicle simulation. J Power Sources 256:410–423. https://doi.org/10.1016/j.jpowsour.2014.01.057
6. Rahman MA, Anwar S, Izadian SA (2016) Electrochemical model parameter identification of a lithium-ion battery using particle swarm optimization method. J Power Sources 307:86–97. https://doi.org/10.1016/j.jpowsour.2015.12.083
7. Botte GG, Subramanian VR, White RE (2000) Mathematical modeling of secondary lithium batteries. Electrochim Acta 45:2595–2609. https://doi.org/10.1016/s0013-4686(00)00340-6
8. Doyle M, Fuller TF, Newman J (1993) Modeling of galvanostatic charge and discharge of the lithium/polymer/insertion cell. J Electrochem Soc 140:1526–1533. https://doi.org/10.1149/1.2221597
9. Fuller TF, Doyle M, Newman J (1994) Simulation and optimization of the dual lithium ion insertion cell. J Electrochem Soc 141:1–10. https://doi.org/10.1149/1.2054684
10. Doyle M, Fuller TF, Newman J (1994) The importance of the lithium ion transference number in lithium/polymer cells. Electrochim Acta 39:2073–2081. https://doi.org/10.1016/0013-4686(94)85091-7
11. Doyle M, Newman J (1995) The use of mathematical modeling in the design of lithium/ polymer battery systems. Electrochim Acta 40:2191–2196. https://doi.org/10.1016/0013-4686(95)00162-8
12. Newman J, Thomas-Alyea KE (2004) Electrochemical systems, 3rd edn. John Wiley & Sons
13. Fuller, TF, Newman, JA (1989) Concentrated solution theory model of transport in solid–polymer–electrolyte fuel cells. In: R. E. White and A. J (eds.), Proceedings of The Symposium on Fuel Cells. Appleby, Proc. Vol. 89-14. Electrochem Soc Proc
14. Lamorgese A, Mauri R, Tellini B (2018) Electrochemical-thermal P2D aging model of a LiCoO2/graphite cell: Capacity fade simulations. Journal of Energy Storage 20:289–297. https://doi.org/10.1016/j.est.2018.08.011
15. Murbach MD, Schwartz DT (2017) Extending Newman's pseudo-two-dimensional lithium-ion battery impedance simulation approach to include the nonlinear harmonic response. J Electrochem Soc 164:E3311. https://doi.org/10.1149/2.0301711jes
16. Subramanian VR, Boovaragavan V, Ramadesigan V, Arabandi M (2009) Mathematical model reformulation for lithium-ion battery simulations: galvanostatic boundary conditions. J Electrochem Soc 156:A260. https://doi.org/10.1149/1.3065083
17. Ramadesigan V, Boovaragavan V, Subramanian VR (2009) Efficient reformulation of solid-phase diffusion in physics-based lithium-ion battery models, ECS Transactions. https://doi.org/10.1149/1.3115314
18. Rahimian SK, Rayman S, White RE (2013) Extension of physics-based single particle model for higher charge–discharge rates. J Power Sources 224:180–194. https://doi.org/10.1016/j.jpowsour.2012.09.084
19. Guo M, White RE (2012) An approximate solution for solid-phase diffusion in a spherical particle in physics-based Li-ion cell models. J Power Sources 198:322–328. https://doi.org/10.1016/j.jpowsour.2011.08.096
20. Santhanagopalan S, Guo Q, Ramadass P, White RE (2006) Review of models for predicting the cycling performance of lithium ion batteries. J Power Sources 156:620–628. https://doi.org/10.1016/j.jpowsour.2005.05.070
21. Subramanian VR, Tapriyal D, White RE (2004) A boundary condition for porous electrodes. Electrochem Solid-State Lett 7:A259–A263. https://doi.org/10.1149/1.1773751
22. Guduru A, Northrop PW, Jain S, Crothers AC, Marchant TR, Subramanian VR (2012) Analytical solution for electrolyte concentration distribution in lithium-ion batteries. J Appl Electrochem 42:189–199. https://doi.org/10.1007/s10800-012-0394-4
23. Johan MR, Arof AK (2007) Modeling of electrochemical intercalation of lithium into a $LiMn_2O_4$ electrode using Green function. J Power Sources 170:490–494. https://doi.org/10.1016/j.jpowsour.2007.03.069
24. Johan MR, Arof AK (2004) Analytical solution to the material balance equation by integral transform for different cathode geometries. Ionics. 10:405–414. https://doi.org/10.1007/bf02378001
25. Ali SH, Hussin A, Arof A (2002) Short- and long-time solutions for material balance equation in lithium-ion batteries by Laplace transform. J Power Sources 112:435–442. https://doi.org/10.1016/s0378-7753(02)00420-2

26. Smith KA, Rahn CD, Wang C-Y (2008) Model Order Reduction of 1D diffusion systems via residue grouping. J Dyn Syst Meas Control 130(011012):1–8. https://doi.org/10.1115/1.2807068
27. Subramanian VR, Ritter JA, White RE (2001) Approximate solutions for galvanostatic discharge of spherical particles I. Constant diffusion coefficient. J Electrochem Soc 148. https://doi.org/10.1149/1.1409397.
28. Luo W, Lyu C, Wang L, Zhang L (2013) An approximate solution for electrolyte concentration distribution in physics-based lithium-ion cell models. Microelectron Reliab 53:797–804. https://doi.org/10.1016/j.microrel.2012.11.002
29. Cai L, White RE et al (2009) J Electrochem Soc 156. https://doi.org/10.1149/1.3049347
30. Carr EJ, Turner IW (2016) A semi-analytical solution for multilayer diffusion in a composite medium consisting of a large number of layers. Appl Math Model 40:7034–7050. https://doi.org/10.1016/j.apm.2016.02.041
31. Choobineh L, Jain A (2015) An explicit analytical model for rapid computation of temperature field in a three-dimensional integrated circuit (3D IC). Int J Therm Sci 87:103–109. https://doi.org/10.1016/j.ijthermalsci.2014.08.012
32. Rodrigo MR, Worthy AL (2016) Solution of multilayer diffusion problems via the Laplace transform. Aust J Math Anal Appl 444:475–502. https://doi.org/10.1016/j.jmaa.2016.06.042
33. Hickson RI, Barry SI, Mercer GN (2009) Critical times in multilayer diffusion. Part 1: Exact solutions. Int J Heat Mass Transf 52:5776–5783. https://doi.org/10.1016/j.ijheatmasstransfer.2009.08.013
34. Pérez Guerrero JS, Pontedeiro EM, van Genuchten MT, Skaggs TH (2013) Analytical solutions of the one-dimensional advection–dispersion solute transport equation subject to time-dependent boundary conditions. Chem Eng J 221:487–491. https://doi.org/10.1016/j.cej.2013.01.095
35. Carr EJ, March NG (2018) Semi-analytical solution of multilayer diffusion problems with time-varying boundary conditions and general interface conditions. Appl Math Comput 333:286–303. https://doi.org/10.1016/j.amc.2018.03.095
36. Parhizi M, Pathak M, Jain A (2020) Analytical model based prediction of state-of-charge (SoC) of a Lithium-ion cell under time-varying charge/discharge currents. J Electrochem Soc 167(120544):1–10. https://doi.org/10.1149/1945-7111/abb34d
37. Liu S (2006) An analytical solution to Li/Li insertion into a porous electrode. Solid State Ionics 177:53–58. https://doi.org/10.1016/j.ssi.2005.09.053
38. Parhizi M, Jain A (2021) Analytical modeling of solution phase diffusion in porous composite electrodes under time-dependent flux boundary conditions using Green's function method. Ionics. 27:213–224. https://doi.org/10.1007/s11581-020-03777-1
39. Parhizi M, Jain A (2020) Analytical modeling of solid phase diffusion in single-layer and composite electrodes under time-dependent galvanostatic flux boundary condition. J Electrochem Soc 167:1–11. https://doi.org/10.1149/1945-7111/ab847c
40. Zhou L, Parhizi M, Jain A (2021) Theoretical analysis of transient solution phase concentration field in a porous composite electrode with time-dependent flux boundary condition. J Appl Electrochem 51:1241–1252. https://doi.org/10.1007/s10800-021-01573-x
41. Krishnan G, Parhizi M, Pathak M, Jain A (2021) Solution phase limited diffusion modeling in a Li-ion cell subject to concentration-dependent pore wall flux. J Electrochem Soc 168:1–9. https://doi.org/10.1149/1945-7111/ac1cfb